Available online at www.sciencedirect.com
SCIENCE DIRECT®
Pergamon
Materials Research Bulletin 38 (2003) 41–54
Materials Research Bulletin
www.elsevier.com/locate/matresbu

Combustion synthesis of $CuFe_2O_4$

R. Kalai Selvan[a], C.O. Augustin[b], L. John Berchmans[b], R. Saraswathi[a,*]

[a]*Department of Materials Science, Madurai Kamaraj University, Madurai 625021, India*
[b]*Central Electrochemical Research Institute, Karaikudi 630006, India*

Received 26 April 2002; received in revised form 22 July 2002; accepted 15 October 2002

Abstract

Metallic ferrites are investigated as prospective materials for different applications especially as anodes in extractive metallurgy. $CuFe_2O_4$, one of the important ferrites, is envisaged for substituting the carbon anode in Hall–Heroult cells. A single step combustion process has been used for the synthesis of $CuFe_2O_4$ powder from cupric nitrate, ferric nitrate and urea. The experimental conditions for maximum conversion efficiency of the precursor powders have been optimized. X-ray diffraction (XRD), Fourier transform infrared spectroscopy (FTIR) and scanning electron microscopy (SEM) have confirmed the formation, structure and homogeneity of the as-prepared powders. The detailed physical, electrical and structural characterization of the materials have been carried out for the specimens obtained on sintering at different temperatures up to 1000 °C.

Keywords: Oxides; Chemical synthesis; X-ray diffraction; Electrical properties; Microstructure

1. Introduction

Advancement of science and technology demands tailor made materials to satisfy specific requirements of the area of applications. Metallic oxides are an important class of compounds and among them ferrites are most prominent by virtue of their spinel structure with high thermodynamic stability, electrical conductivity, electro-catalytic activity and resistance to corrosion. They are widely used in computer peripherals, telecommunication equipments, permanent magnets, electronic and microwave devices [1]. Ferrites of Co, Zn and Ni were studied as electrodes for oxygen evolution in molten salt systems [2–5]. Molten salts are very sensitive and complicated systems, maintained at high temperatures, where only few materials can thrive efficiently. Recently, Aluminum company of America (Alcoa) supported by US Department of Energy, carried out significant work on ferrites [6]. A review of new materials for the use in aluminum production with an emphasis on electrode materials

* Corresponding author. Tel.: +91-452-458247; fax: +91-452-459181.
E-mail address: saraswathir@yahoo.com (R. Saraswathi).

0025-5408/02/$ – see front matter
PII: S0025-5408(02)01004-8

has been published [7]. Some studies have been carried out on pure and substituted $CuFe_2O_4$ by electrochemical [8] and ceramic methods [9,10]. Mahajan and coworkers [11] have carried out thermoelectrical and electrical measurements on $CuFe_2O_4$. The phase transition studies of this compound have been done by Murthy et al. [12]. Mazen et al. [13] have studied the thermal and electrical properties of this material.

In this context $CuFe_2O_4$ assumes great significance because of its high electronic conductivity, high thermal stability and high catalytic activity for O_2 evolution from alumina–cryolite system used for aluminum production. The novelty and importance of the new applications of $CuFe_2O_4$ lie in the fact that it serves as a non-consumable and green anode for aluminum electrolysis. The significance is that at $CuFe_2O_4$ anode, only oxygen gas is evolved instead of CO_2—a green house gas evolved at the widely used carbon anode.

In this investigation, a single step combustion process [14] has been adapted to synthesize $CuFe_2O_4$ powder. The combustion synthesis (CS) is an efficient method for the preparation of new oxide materials. The attractive features of CS are its ability to synthesize materials with high purity, better homogeneity and high surface area in a single step. A detailed characterization covering the particle size, density, porosity, ac and dc electrical conductivity and structural properties have been reported in this paper.

2. Experimental

2.1. Synthesis

For the combustion synthesis of copper ferrite powder, $Cu(NO_3)_2{\cdot}3H_2O$ and $Fe(NO_3)_3{\cdot}9H_2O$ were used as cation precursors and $CO(NH_2)_2$ was used as fuel. The reactants were dissolved in a minimum quantity of deionized water in a cylindrical Pyrex dish. The dish containing the solutions was placed on an heater maintained at around 300 °C. Initially the solution boiled and underwent dehydration followed by decomposition with evolution of copious amounts of heat and gases. The mixture then frothed and swelled forming foam, which ruptured with a flame and finally gave foamy powder of copper ferrite, which is labeled as ‘a’.

2.2. Particle size analysis

The finely ground copper ferrite powders were analyzed by Laser particle size analyzer (model MALVERN 3600 EC, England). The transmitting source is He–Ne laser of 362.8 nm wavelength. The complete range of particle size distribution measurement is 0.5–560 μm.

2.3. Compacting

The powders were thoroughly ground and slowly filled up in the die and pressure was applied for 2 min. The individual blends were compacted to 3.5 tons cm^{-2} and the pellets were plunged from the die. A large number of pellets of two sizes (1 and 2.5 cm diameter) were compacted under identical conditions. A West Germany make hydraulic press of 64 tons capacity was used to compact the pellets.

2.4. Sintering

Sintering is a process to treat the material at high temperatures. The compacts were placed in an electrically heated furnace fitted with digital temperature controller cum-indicator and heated continuously up to 1000 °C, holding at an intermediate temperature of 700 °C for long duration. The sample sintered at 700 °C is labeled as 'b' and that at 1000 °C as 'c'.

2.5. Density

A known amount of powder sample was filled into a graduated cylinder of 10 ml capacity. The cylinder was tapped until the powder level remained unchanged. The volume occupied by the powder was noted. The ratio between the weight of the sample and volume gave tap density.

The powder densities were measured using Archimedes principle with a pycnometer and xylene as a liquid medium. A pycnometer of volume 25 ml was used. The following relationship was used to calculate the density of the sample:

$$\rho = \frac{W_2 - W_1}{(W_4 - W_3) + (W_2 - W_1)} \times \rho_{\text{sol}} \tag{1}$$

where W_1 is the weight of the bottle (in g), W_2 the weight of the bottle + sample (in g), W_3 the weight of the bottle + sample + xylene (in g), W_4 the weight of the bottle + xylene (in g), and ρ_{sol} is the density of xylene.

The X-ray density of the samples has been calculated from the lattice parameters using the formula

$$D_{hkl} = \frac{8M}{Na^3} \tag{2}$$

where M is the molecular weight of the sample, N the Avogadro's number and a is the lattice parameter of the sample.

2.6. Porosity

The porosity of the pellet was obtained by liquid absorption method. In this method, a non-reactive liquid like glycerol (density = 1.261 g cm^{-3}) is used to fill up the pores under vacuum. From the weight of the liquid entered into the pellet the volume can be calculated from the known density and subsequently the porosity (P) of the material can be computed by the following relationship:

$$P\,(\%) = \frac{\Delta W}{d} \times \frac{1}{\pi r^2 h} \times 100 \tag{3}$$

where ΔW is the weight of the glycerol absorbed, d the density of glycerol, r the radius of the pellet and h is the height of the pellet.

2.7. Electrical conductivity

The frequency variations of ac conductivity of all samples were carried out at room temperatures from 50 to 10 kHz with the help of computerized LCRTZ systems (model VLCRTZ1P). For better

ohmic contact in these measurements silver paste was applied to both surfaces of the pellet before being sandwiched between the two electrodes of sample holder.

The dc electrical conductivity was measured as a function of temperature of the sintered specimens using the modified four probe method. Pt wires were used as current and potential leads and measurements were carried out from ambient temperature to 1000 °C. The resistance was measured by digital micro-ohmmeter and the measurements were repeated for all samples with heating and cooling cycles and the error was found to be less than 1%. Temperature near the samples was measured using Cr–Al thermocouple and the temperature programmer controlled the rate of heating.

2.8. Optical studies

The X-ray powder diffraction patterns of green and sintered specimens were recorded using Cu Kα ($\alpha = 1.541$ Å) radiation with 2θ value ranging from 20 to 90° in JEOL 8030 X-ray diffractometer.

The FTIR spectra of the samples were recorded as KBr discs in the range 400–1000 cm^{-1} by using FTIR–Perkin-Elmer, UK Paragon-500.

A Japan made scanning electron microscope (SEM) JEOL (JSM—3.5 CF) instrument was used for the morphological studies.

3. Results and discussion

3.1. Combustion synthesis

The copper ferrite is synthesized by the combustion route, using urea as fuel, crystalline Cu $(NO_3)_2{\cdot}3H_2O$ as a Cu source (total valencies: −10) and $Fe(NO_3)_3{\cdot}9H_2O$ as a Fe source (total valencies: −15). The combustion synthesis technique is based on the thermochemical concepts used in propellant chemistry [15], in which different fuels such as tetraformyl triazine TFTA ($C_4H_{16}N_6O_2$), maleic hydrazide ($C_4H_4N_2O_2$), carbohydrazide ($CO(N_2H_3)_2$) and glycine (NH_2CH_2COOH) have been used. All of these fuels contain nitrogen but differ in the reducing power and the amounts of gases that generate, which obviously affects the characterization of the reaction product. The advantages of urea are that it has the lowest reducing power (total valencies: +6), cheap, commercially available and produces the smallest volume of gases. The nitrate salts are favored as precursors because they serve as water-soluble low temperature nitrogen source for the synthesis. The enthalpy change involved in the various chemical reactions can be calculated from the published thermodynamic data [16] listed in Table 1. Table 2 enumerates the various chemical reactions involved in the synthesis of copper ferrite. The combustion reaction of urea, described by the equation R1 in Table 2, is exothermic and should provide the heat needed for the $CuFe_2O_4$ synthesis reaction. The decompositions of the individual metal nitrate salts are given by reactions R2 and R3. RS2 = RS1 + mR1 (Table 2) gives the overall synthesis reaction. For this reaction RS2 to occur at 25 °C, $m = 3.1904$ mol of urea is needed solely on the basis of enthalpy change ($\Delta H^{\circ}_{RS2} = 0$). This amount of urea satisfies the enthalpy requirement for complete decomposition at 25 °C and the release of all the corresponding gases ($27.38H_2O\uparrow + 7.19N_2\uparrow + 10O_2\uparrow + 3.19CO_2\uparrow$), as predicted by reaction RS2.

Since the anticipated temperature is not sufficient to bring out the synthesis, direct use of the propellant chemistry, with the metal nitrates in 1:2 molar ratio, to determine the urea needed to balance

Table 1
Thermodynamic data for related compounds

Compound	ΔH_f° (25 °C) (kcal mol^{-1})	ΔH_f° (25 °C) (kcal mol^{-1})	S (25 °C) (cal mol^{-1} K^{-1})	C_p (25 °C) (cal mol^{-1} K^{-1})
$Cu(NO_3)_2{\cdot}3H_2O$(c)	−288.55	206.5		
$Fe(NO_3)_3{\cdot}9H_2O$(c)	−785.2	591.087		
$CO(NH_2)_2$(c)	−79.71	−47.04	25	22.26
$CuFe_2O_4$(c)	−230.69	−205.26	33.7	35.52
Fe_2O_3(c)	−198.5	−177.4	20.89	24.82
CuO(c)	−37.6	−31	10.19	10.11
FeO(c)	−64.62	−60.10	14.52	11.93
Fe_3O_4(c)	−266.9	−242.7	35	35.19
Cu_2O(c)	−43.3	−34.9	22.26	15.21
H_2O(l)	−68.3174	−56.643	16.723	17.98
H_2O(g)	−57.796	−54.634	45.104	$7.2 + 0.0036T$[a]
CO_2(g)	−94.051	−94.26	51.07	$10.34 + 0.00274T$[a]
N_2(g)	0	0	45.77	$6.5 + 0.00100T$[a]
O_2(g)	0	0	49.003	$5.92 + 0.00367T$[a]
NO(g)	21.57	20.69	50.349	$6.46 + 0.00179T$[a]
NO_2(g)	7.96	12.25	57.35	8.887
N_2O(g)	19.55	24.89	32.53	9.1976

c: crystalline; g: gas; l: liquid; T: absolute temperature.
[a] Calculated for discrete values.

the total oxidizing and reducing valencies in the mixture of oxidizer and fuel leads to $(-10) + 2(-15) + n(+6) = 0$. Thus, the stoichiometric composition of the redox mixture, required to release the maximum energy for the reaction, demands that $n = 6.67$ mol of urea, so as to get a molar proportion of 1:2:6.67. The combustion of the extra 3.48 mol of urea specified by the propellant chemistry calculations will consume all the released oxygen and the heat generated will be absorbed by the resulting gases ($6.9592H_2O\uparrow + 3.4796N_2\uparrow + 3.4796CO_2\uparrow$), the gases already present and the single oxides, raising their temperature [17]. In such a thermally isolated system, the temperature to which the product is raised can be considered as an adiabatic temperature T_{ad}. The enthalpy of the

Table 2
Chemical reactions involved in the combustion synthesis

Reaction	Descriptive equation	ΔH_f° (25 °C) (kcal mol^{-1})
R1	$CO(NH_2)_2(c) + 1.5O_2(g) \Rightarrow CO_2(g) + 2H_2O(g) + N_2(g)$	−129.9
R2	$Fe(NO_3)_3 \cdot 9H_2O(c) \Rightarrow 0.33Fe_3O_4(c) + 9H_2O(g) + 1.5N_2(g) + 3.83O_2(g)$	176.959
R3	$Cu(NO_3)_2 \cdot 3H_2O(c) \Rightarrow CuO(c) + 3H_2O(g) + N_2(g) + 2.5O_2(g)$	78.162
R4	$CuO(c) + Fe_2O_3(c) \Rightarrow CuFe_2O_4(c)$	5.41
RS1	$Cu(NO_3)_2 \cdot 3H_2O(c) + 2Fe(NO_3)_3 \cdot 9H_2O(c) \Rightarrow CuFe_2O_4(c) + 21H_2O(g) + 10O_2(g) + 4N_2(g)$	414.544
RS2	$Cu(NO_3)_2 \cdot 3H_2O(c) + 2Fe(NO_3)_3 \cdot 9H_2O(c) + mCO(NH_2)_2(c) + 1.5O_2(g) \Rightarrow CuFe_2O_4(c) + (21 + 2m)H_2O(g) + (4 + m)N_2(g) + 10O_2(g) + mCO_2(g)$	$414.544 - 129.933m$

c: crystalline; g: gas; l: liquid.

reaction can be expressed as

$$\Delta H^{\circ}_{298} = \int_{298}^{T_{ad}} C_p(\text{product})\,dT \tag{4}$$

where ΔH_{298} is the enthalpy of the reaction at 298 K, C_p(product) the heat capacity of the product and T_{ad} is the adiabatic temperature to which the reaction system is raised

$$Q = -\Delta H^{\circ}_{298} = \int_{298}^{T_{ad}} C_p(\text{product})\,dT \quad (\Delta H^{\circ}_{298} = -452.09\,\text{kJ/mol}, \quad T_{ad} = 1239\,\text{K}) \tag{5}$$

This temperature is sufficient to form the copper ferrite phase, which is comparable to the experimental value 1150 K. Hence, the combustion synthesis technique proves to be a much simple and more efficient route to synthesize copper ferrite compound, in line with the earlier investigations carried out on other perovskites, spinels and oxide materials [18–20].

3.2. Characterization

The particle size of the prepared copper ferrite is found to have a bearing on the compacting characteristic and also on the improvement of properties. The particle size was found to be 6.3 μm and specific surface area was found to be 0.68 $m^2\,ml^{-1}$, which show that a uniform product has been formed in the combustion process and thorough homogenization was obtained in the chemical reaction resulting in the synthesis of new phase of copper ferrite.

Table 3 shows the density and porosity values for the all the samples. The relative gain in density with raise in temperature from RT to 1000 °C is found to be more in the case of powder than in the pellet, inferred from the ratio of 2.38 and 1.76, respectively. The improvement in density is due to the cohesive binding and rearrangement of atoms realized from the effect of both pressure and temperature. Porosity, which is a measure of the empty space within the pellet, is found to be more at low temperature as can be seen from Table 3. The porosity at 1000 °C decreases to about 40% of the value at 31 °C. The decrease in porosity may be due to the pore elimination, reorientation and transport of materials from different centers.

Fig. 1 provides the ac conductivity versus frequency for the green and sintered specimens at temperatures of 700 and 1000 °C. As the frequency increases the conductivity is found to increase for all the samples but a rapid rate of increase in conductivity is observed at low frequency value, which tends to become almost constant at 10 kHz. This is an established normal behavior of ferrite materials [21,22]. A discrepancy is observed for the material sintered at 1000 °C having a lower conductivity for all frequencies than the material sintered at 700 °C. Among all the samples the highest ac conductivity recorded was 14×10^{-4} S cm^{-1}. Similarly the relationship between $\log(\sigma_{ac} - \sigma_{dc})$ versus $\log(\omega^2)$ is

Table 3
Physical properties of the sample

Sample	Tap density (g cm^{-3})	Pellet density (g cm^{-3})	X-ray density (g cm^{-3})	Porosity (%)
Green	1.47	2.7	5.536	28
700 °C	1.60	3.03	5.585	18.5
1000 °C	3.509	4.756	5.674	14.5

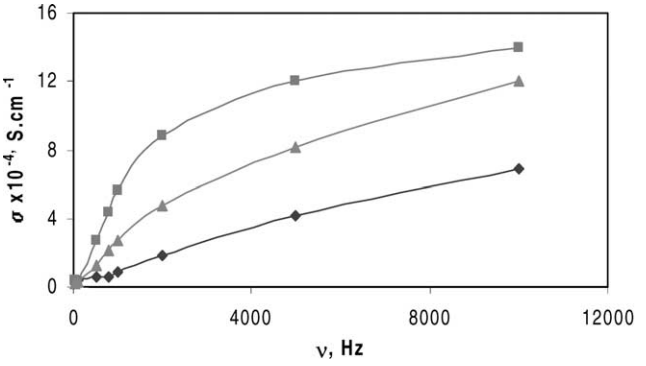

Fig. 1. Plot of ac conductivity vs. frequency for (◆) green, (■) 700 °C and (▲) 1000 °C.

given in Fig. 2. A straight-line graph resulted for all the materials and hence the behavior is found to be linear at all conditions, which is indicative of conduction by small polarons. The reason for the discrepancy may be due to the presence of uncommon valency of copper especially Cu^{+} ions. Further the occupation of identical lattice points with Cu^{+} and Cu^{2+} ions makes the behavior more unusual. The Cu^{+} ions is made available by the reduction of Cu^{2+} ions which in turn makes excess holes and the in situ generation of p-type conductivity in the material. Secondly a polarization phenomenon due to the ferrous–ferric interchange can also be attributed to the anomaly. In general electronic exchange between Fe^{2+} and Fe^{3+} at similar positions are favored while the structures are oscillating from one to another. It is known that the effect of polarization is to reduce the field inside the medium. Therefore, the ac conductivity of the sample was increased by the increase in frequency.

The specific conductivity (σ) was obtained by resistance measurements as a function of temperatures (Fig. 3). It can be seen that dc electrical conductivity increases with increasing temperature for both the samples sintered at 700 and 1000 °C [23], but a rapid increase in σ is observed above 800 °C for the sample sintered at 1000 °C.

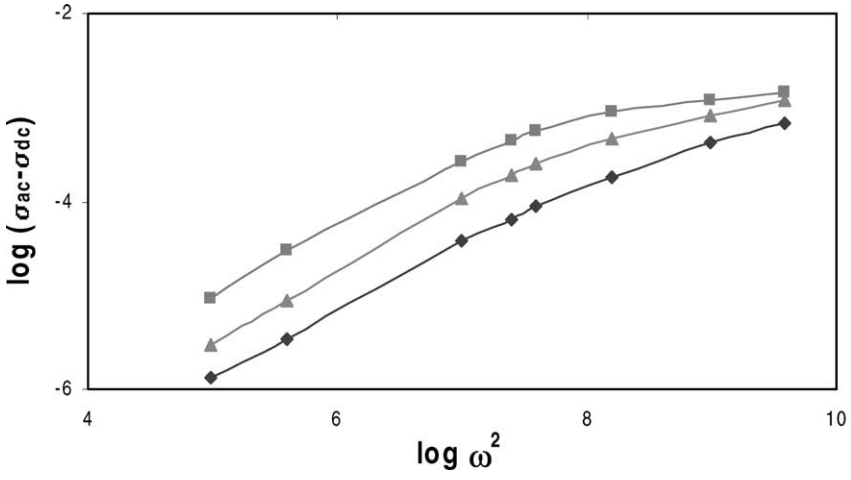

Fig. 2. Plot of $\log(\sigma_{ac} - \sigma_{dc})$ vs. $\log(\omega^2)$ for (◆) green, (■) 700 °C and (▲) 1000 °C.

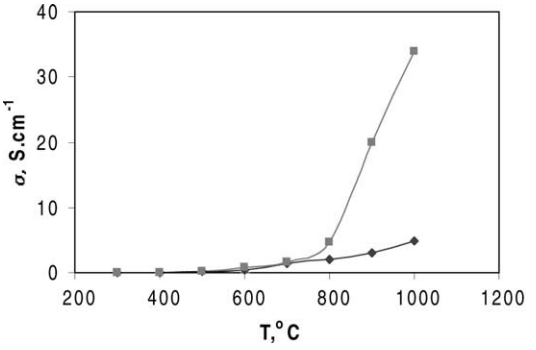

Fig. 3. Plot of dc conductivity vs. temperature for (◆) 700 °C and (■) 1000 °C.

The specific conductivity values for the above sintered materials are 4.85 and 34 S cm^{-1}, respectively at 1000 °C. From these observations, we conclude that the sintering temperature has a positive effect on the electrical conductivity. No doubt measuring temperature also has some influence on the conductivity, but it has a less pronounced effect compared to the sintering temperature.

The electrical conduction in spinel ferrite is due to the transfer of electrons between Fe at different valencies, i.e. Fe^{2+} and Fe^{3+}. The nature of the conductivity values shows the dependence of conductivity mainly on temperature-assisted mobility rather than on the carrier concentration. The very low conductivity value of 2×10^{-4} S cm^{-1} at 300 °C for the material sintered at 700 °C itself indicates that the conductivity of the powder at room temperature will be in the lower range of semiconductivity. As the materials are sintered, the copper ferrite is subjected to various internal changes governed by the thermal interactions, prominent being the increase in the carrier species especially the Cu^{2+}, Fe^{2+} and Fe^{3+} ions. The temperature will also increase the concentration of the species but their contribution towards the net conduction may be low in comparison with mobility. The dependence of the dc resistivity of the material on the temperature is given by the Arrhenius relationship:

$$\rho = \rho_0 \exp\left(\frac{\Delta E}{KT}\right) \tag{6}$$

where ρ is the specific resistivity at T K, ρ_0 the specific resistivity at absolute zero temperature, E the activation energy and K is the Boltzmann constant.

The Arrhenius plot (Fig. 4) gives the different regions indicative of different types of electrical behavior. At low temperature a higher resistance is observed which may be the result of large number of voids and less cohesion. But the low resistance at high temperature is due to polaron hopping. It is reported that copper ferrite acts both as n- and p-type semiconductors [24,25]. The two competing mechanisms may be due to the following redox reactions:

$$Fe^{2+} \Leftrightarrow Fe^{3+} + e^{-} \tag{7}$$

$$Cu^{2+} \Leftrightarrow Cu^{+} + e^{+}\,(\text{hole}) \tag{8}$$

By combining Eqs. (7) and (8)

$$Fe^{2+} + Cu^{2+} \Leftrightarrow Fe^{3+} + Cu^{+} \tag{9}$$

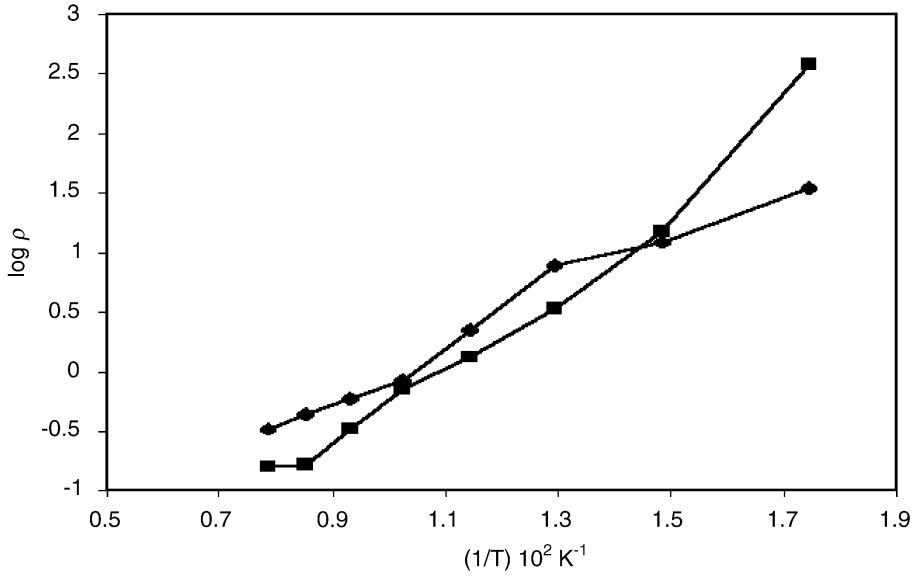

Fig. 4. Plot of log ρ vs. $(1/T) \times 10^3$ for (●) 700 °C and (▲) 1000 °C.

The type of carriers and their concentrations are decided by the kinetics of the reactions. According to Eq. (7), the current carriers are mostly electrons generated from Fe^{2+} centers, which act as electron donors in an electron-hopping model [26]. The electron hopping occurs by electron transfer between adjacent octahedral sites in the spinel lattice [27]. Thus, at elevated temperature the fractions of Fe^{2+} and the availability of electrons will be much more than at low temperature. At lower temperature the conduction is due to extrinsic type while at higher temperature due to polaron hopping [10]. The conduction mechanism of $Cu_xFe_{3-x}O_4$ has been studied elaborately by Patil et al. [11]. The break in the Arrhenius plot is due to the change in conducting mechanism. A change in slope can be attributed to two parallel conductivity mechanisms with different activation energies [28]. It is observed that the values are different for different regions. The activation energies for sample 'b' are 0.93 and 0.41 eV whereas 0.9, 0.4 and 0.6 eV for sample 'c'. From Fig. 4, the Curie temperature is 709 K on sample 'c', which agrees with the earlier reported values of 670–750 K [29]. Moreover, the activation energies of the material are greater than 0.4 eV, which clearly suggest that the conduction is due to polaron hopping [30].

The X-ray diffraction (XRD) pattern of copper ferrite sample is shown in Fig. 5a–c. Sharp and well-defined peaks are obtained for all the samples. The XRD pattern for green sample gives CuO, Fe_2O_3 and $CuFe_2O_4$ peaks, while at 700 °C the intensities of the lines have increased. Further sintering of the material at 1000 °C helps to increase the percentage of $CuFe_2O_4$ to almost 100%, evident from the prominent peaks emanated from the '*hkl*' planes (2 2 0), (1 1 3), (4 0 0) and (4 4 0). The presence of single phase $CuFe_2O_4$ has been further confirmed by the absence of CuO and Fe_2O_3 peaks in Fig. 5c. The '*d*' spacing for the recorded peaks are calculated according to Bragg's law. The lattice parameters for the 1000 °C-sintered sample were found to be $a = 8.208$ Å, $c = 8.621$ Å and $c/a = 1.05$ Å. The reported values for '*c*/*a*' lie between 1.01 and 1.06 Å for copper ferrite sample prepared by various methods [9,20,31]. These values are in close proximity with our values, which also confirms a

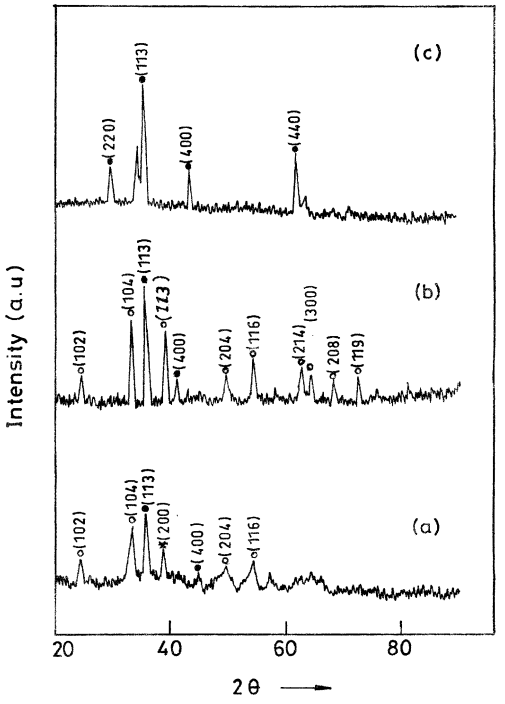

Fig. 5. XRD pattern of $CuFe_2O_4$: (a) green, (b) 700 °C and (c) 1000 °C sample.

tetragonal structure for the synthesized copper ferrite. Moreover, the Cu^{2+} is a Jahn–Teller ion and can distort to give a tetragonal crystal system [32].

The percentage of phase formation is summarized in Table 4. The phase formation is estimated from the relation

$$\text{Percentage of copper ferrite} = \frac{I_{CFO}}{I_{CO} + I_{FO} + I_{CFO}} \tag{10}$$

where I_{CFO} is the maximum intensity of $CuFe_2O_4$ peak, I_{CO} the maximum intensity of CuO peak and I_{FO} is the maximum intensity of Fe_2O_3 peak.

The FTIR spectra for the copper ferrite samples were recorded in the range of 400–1000 cm^{-1} and are shown in Fig. 6a–c for green, 700 and 1000 °C-sintered samples, respectively. These spectra show two main absorption bands γ_1^* and γ_2^* as common feature of all spinel compounds, in accordance to

Table 4
XRD data of copper ferrite

Sample	d_{400} (Å)	a (Å)	d_{113} (Å)	c (Å)	c/a	Cell volume (Å)	Phase formation (%)		
							CuO	Fe_2O_3	$CuFe_2O_4$
Green	2.013	8.052	2.506	8.372	1.03	542.79	26.5	35.6	37.8
700 °C	2.174	8.696	2.657	8.838	1.01	668.33	–	44.7	55.22
1000 °C	2.052	8.208	2.576	8.621	1.05	580.80	–	–	100

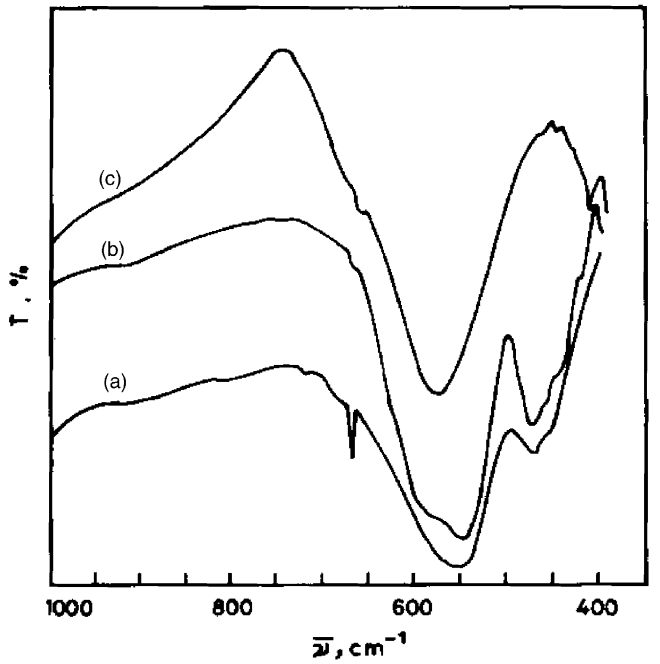

Fig. 6. FTIR pattern of $CuFe_2O_4$: (a) green, (b) 700 °C and (c) 1000 °C sample.

Waldron [33]. The ferrite can be considered as continuously bonded crystals, via ionic, covalent or van der Walls forces, to the nearest neighbors. In ferrite the metal ions are situated in two different sublattices, namely tetrahedral (A sites) and octahedral (B sites) according to the geometrical configuration of the oxygen nearest neighbors. The band γ_1^* around 600 cm^{-1} is attributed to stretching vibration of tetrahedral complexes and the band γ_2^* around 400 cm^{-1} to that of octahedral complexes. The values of the absorption band frequency of the green and sintered samples are given in Table 5. It can be seen that the high frequency band γ_1^* has a value 553.57 cm^{-1} for green sample, 546.26 cm^{-1} for 700 °C-sintered sample and 578.12 cm^{-1} for 1000 °C-sintered sample. The lower frequency band γ_2^* is 467.11, 474.93 and 420.34 cm^{-1} for green, 700 and 1000 °C samples, respectively. These values agree with the earlier observations [34] in which γ_1^* becomes 597 and 415 cm^{-1} is a γ_2^*. The sample was prepared by 'Chimie douce' method via decomposition of mixed oxalate precursors. In inverse ferrites such as copper ferrite, the γ_1 band is due to Fe^{3+}–O^{2-} complex present at A sites and the γ_2 band due to vibrations of

Table 5
FTIR parameters

Sites	Band (cm^{-1})	Green (cm^{-1})	700 °C (cm^{-1})	1000 °C (cm^{-1})	Me–O^{2-}
Tetrahedral sites (A-sites)	γ_1^*	553.57	546.26	578.12	Fe^{3+}–O^{2-}
	γ_1'	668.06	600	680	Cu^{2+}–O^{2-}
Octahedral sites (B-sites)	γ_2^*	467.11	474.93	420.34	
Threshold frequency	γ_{th}	735	760	780	Fe^{3+}–O^{2-}
Threshold energy	E_{th} (eV)	0.092	0.095	0.097	

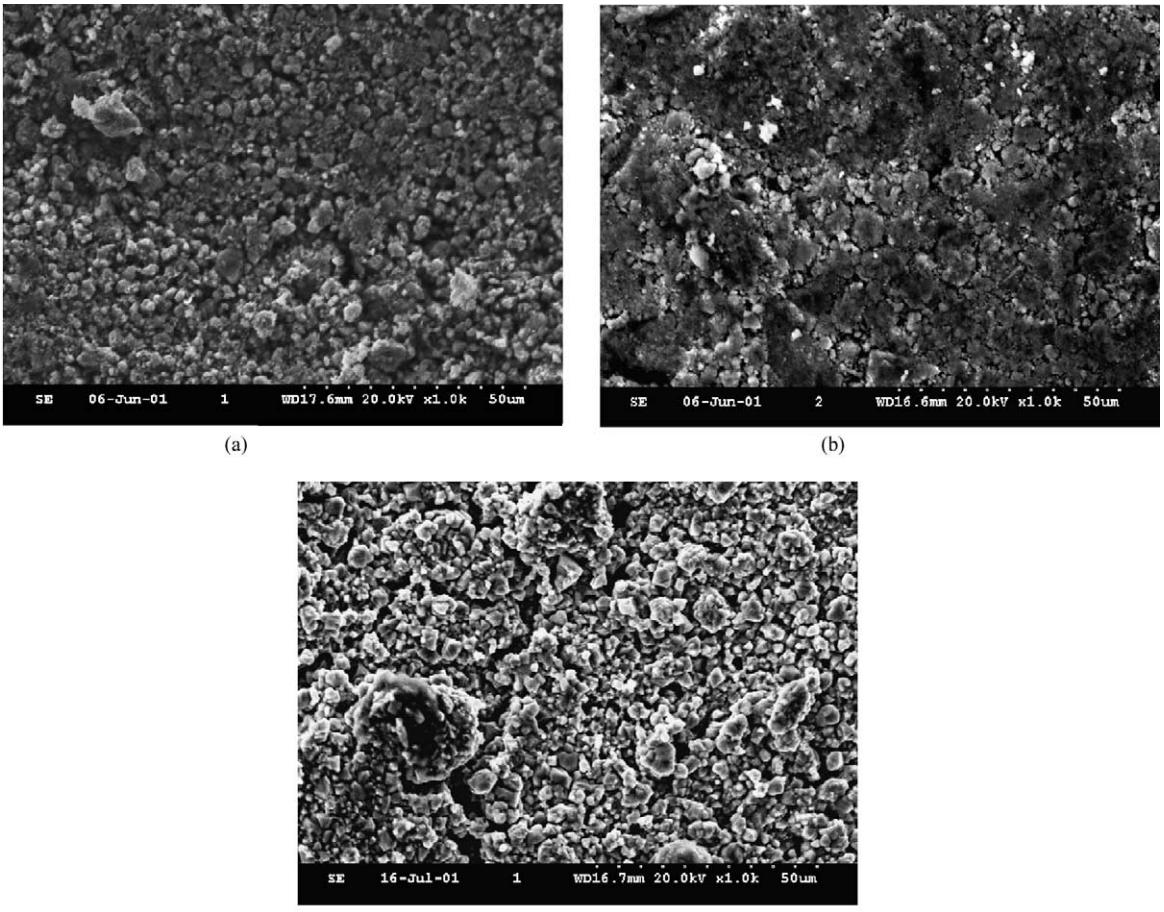

Fig. 7. SEM micrographs of $CuFe_2O_4$: (a) green, (b) 700 °C and (c) 1000 °C sample.

octahedral metal complexes. The Cu^{2+} ions occupy mainly the octahedral sites and some fraction goes into tetrahedral sites. Accordingly, this shoulder can be attributed to the vibration of Cu^{2+}–O^{2-} in tetrahedral complexes. On the basis of the above discussion and on earlier studies [34,35] an inverted spinel structure can be assigned to the copper ferrite. Further, the cation distribution for the synthesized material is suggested to be

$$(Cu_y{}^{2+}Fe_{1-y}{}^{3+})_A[Cu_{1-2y}{}^{2+}Fe_{1+2y}{}^{3+}]_BO_4{}^{2-}$$

The threshold frequency γ_{th} for the electronic transition can be determined from the absorption spectra. It is found that the threshold energy decreases with sintering temperature. The average value of threshold energy is 0.095 eV.

The morphological features of green, 700 and 1000 °C-sintered samples are shown in Fig. 7a–c. The average particle size of the powder is in the range of 8 μm for the green sample. The effect of temperature on the materials is to enhance the agglomeration wherein the particles have increased in size to attain a higher crystallite size of 20 μm. It is also seen that the density has increased further

followed by a decrease in porosity. The overall improvement in the properties of the material may be due to better grain-to-grain connectivity as evident from the microphotographs.

4. Conclusion

The combustion synthesis is observed to be an efficient and convenient method to synthesize new compounds especially copper ferrite. The material has been identified as an inverted spinel with tetragonal structure. From the electrical conductivity data the material is found to be a semiconductor with a band gap value of 0. 4 eV. The synthesized copper ferrite is expected to be a suitable anode material, on the basis of its physical and electrical properties.

Acknowledgements

The authors express their gratitude to the Director, CECRI, and staff of Electro Pyrometallurgy Division and Department of Materials Science, Madurai Kamaraj University, Madurai, for their support.

References

[1] D. Bahadur, Bull. Mater. Sci. 15 (1992) 431.
[2] C.O. Augustin, L.K. Srinivasan, K. Srinivasan, Bull. Electrochem. 9 (1993) 502.
[3] E. Olser, J. Thonstad, J. Appl. Electrochem. 29 (1999) 293.
[4] L. JohnBerchmans, C.O. Augustin, U. Sen, Minerals and metals review, Millennium Issue 26 (2000) 55.
[5] C.O. Augustin, L.K. Srinivasan, A. Mani, J. Mater. Sci. Technol. 12 (1996) 417.
[6] J.D. Weyand, D.H. Deyoung, F.W. Baker (Alcoa Lab, Alcoa Center, 1986) DOE No. DOE/CS/40158-20, Department of Energy, Idaho Falls, ID, 1986.
[7] J.A. Sekhar, J. Liu, H. Deng, V. de Nora, Light metals, in: B. Welch (Ed.), The Minerals, Metals and Materials Society, Warrendale, 1998, p. 597.
[8] S.D. Sartale, C.D. Lokhande, Mater. Chem. Phy. 70 (2001) 274.
[9] S.A. Mazen, Mater. Chem. Phys. 62 (2000) 131.
[10] R.P. Mahajan, K.K. Patankar, S.A. Patil, Bull. Mater. Sci. 23 (2000) 273.
[11] A.N. Patil, R.P. Mahajan, S.A. Patil, Ind. J. Pure Appl. Phys. 38 (2000) 651.
[12] K.S.R.C. Murthy, S. Mahanty, J. Ghose, Mater. Res. Bull. 22 (1987) 1665.
[13] S.A. Mazen, M.A. Ahamad, B.A. Sabrah, Phys. Stat. Sol. A 70 (1982) K71.
[14] K.C. Patil, S.T. Aruna, S. Ekambaram, Curr. Opin. Solid State Mater. Sci. 2 (1997) 158.
[15] S.R. Jain, K.C. Adiga, V.R. Pai verneker, Combust. Flame 40 (1981) 71.
[16] J.A. Dean (Ed.), Lange's Hand Book of Chemistry, 12th ed., McGraw-Hill, New York, 1979.
[17] M.T. Colomer, D.A. Fumo, A.M. Segadaes, J. Mater. Chem. 9 (1999) 2505.
[18] D.A. Fumo, J.R. Jurado, J.R. Frade, Mater. Res. Bull. 42 (1997) 1459.
[19] R.D. Purohit, B.P. Sharma, A.K. Tyagi, Mater. Res. Bull. 36 (2001) 2711.
[20] A.B. Naik, S.A. Patil, J.I. Powar, J. Mater. Sci. 7 (1998) 103.
[21] S.S. Bellad, S.C. Watewe, B.K. Chougule, Mater. Res. Bull. 34 (1999) 1099.
[22] S.S. Bellad, B.K. Chougule, Mater. Chem. Phys. 66 (2000) 58.
[23] C.O. Augustin, D. Prabhakaran, L.K. Srinivasan, J. Mater. Sci. Lett. 12 (1993) 383.
[24] K.K. Patankar, V.L. Mathe, K.V. Siva Kumar, Mater. Chem. Phy. 72 (2001) 23.

[25] M. Rosenberg, P. Nicoloau, I. Bunget, Phys. Stat. Sol. 15 (1966) 521.
[26] R.R. Heikes, W.D. Johnston, J. Chem. Phys. 26 (1957) 582.
[27] G.H. Jonker, J. Phys. Chem. Solids 9 (1959) 105.
[28] O.S. Josyulu, J. Sobhanadri, Phys. Stat. Sol. A 59 (1980) 323.
[29] S.A. Mazen, A. Elfalaky, H.A. Hashem, Appl. Phys. A 61 (1995) 559.
[30] M.I. Klinger, J. Phys. C. 8 (1975) 3595.
[31] W.B. Cross, L. Affleck, Q.A. Pankhurst, J. Mater. Chem. 9 (1999) 2545.
[32] S.A. Patil, S.M. Otari, S.R. Sawant, Solid State Commun. 78 (1991) 39.
[33] R.D. Waldron, Phys. Rev. 99 (1955) 1727.
[34] B. Gillot, V. Nivoix, A. Rousset, Mater. Chem. Phys. 48 (1997) 111.
[35] B.J. Evans, S.S. Hafner, J. Phys. Chem. Solids 29 (1968) 1573.